*Acta Cryst.* (1983). A**39**, 79–83

# Measurement of X-ray Integrated Intensity with Diagnostic Identification of Peak and Background

BY A. MCL. MATHIESON

*CSIRO, Division of Chemical Physics, PO Box* 160, *Clayton, Victoria, Australia* 3168

(*Received* 17 *September* 1981; *accepted* 23 *July* 1982)

## Abstract

Recognition of the intrinsic two-dimensional nature of the intensity distribution, $I(\omega,2\theta)$, of a Bragg X-ray reflexion allows identification of the spectral dispersion of the source and the fragment/mosaicity ($f/m$) distribution of the specimen small crystal. With this information as a basis for the measurement of integrated intensity, the spectral band (wavelength truncation) can be maintained constant from reflexion to reflexion and the real extent of the $f/m$ distribution established by reference to a signal/noise index. With this procedure, the separation of peak from background is placed on an objective basis not feasible with the conventional analysis of the one-dimensional reflexion profile. The method is demonstrated using the $\omega/2\theta$ slice scan procedure [Mathieson (1982). *Acta Cryst.* A**38**, 378–387] but is also relevant to the use of linear position-sensitive detectors.

## Introduction

The measurement of integrated X-ray intensity to be discussed is in relation to a small single crystal mounted on a four-circle diffractometer. The traditional, virtually universal, procedure is based on the use of a relatively wide aperture in front of the detector, the process of measurement yielding a one-dimensional distribution, $I(\omega)$, corresponding to the scan chosen, $\omega$, $\omega/\theta$ or $\omega/2\theta$. This profile is viewed as consisting essentially of two components – the peak and the background. The peak corresponds to the diffraction of the spectral line(s) or spectral band by one *hkl* order while the background corresponds to general scattered radiation which subsumes the peak and is assumed uniform or only changing gradually in the region of the reflexion, *e.g.* Lehmann (1980); Clegg (1981).

In this procedure, one is concerned to try to identify what constitutes the peak and what constitutes the background so that the peak data can be isolated to derive a value of integrated intensity and hence the value of the *hkl* structure factor.

Since the profile distribution arises from projection onto one dimension of the convolution of the various contributing factors and corresponds to a smooth peak function superimposed on a smooth background, the transition from peak to background is virtually impossible to recognize. Various methods of differing complexity have been evolved to handle this problem [see Clegg (1981) for a summary of the various procedures] but essentially the decision as to what is peak and what background has rested on subjective criteria even if these are incorporated into a data-processing routine.

It may therefore be of interest to draw attention to a different approach to the measurement of integrated intensity arising from recognition of the two-dimensional nature of Bragg reflexions, an approach which allows a more objective assessment of peak and background.

The procedure, using a standard scintillation counter, is more elaborate and therefore more time consuming than the traditional one but it has potential for greater accuracy and would become more time effective with a linear position-sensitive quantum counter of suitable spatial resolution.

It is not suggested that this procedure is advisable for routine structure analysis but it would be appropriate for detailed electron density studies, where the highest accuracy is sought.

## Method

In a recent study (Mathieson, 1982) using a narrow slit as aperture in front of a scintillation detector, we have demonstrated the functional dependence of an individual Bragg X-ray reflexion on two variables, the angular setting of the crystal, $\omega$, and that of the detector aperture, $2\theta$. There is, of course, a third parameter – that normal to the plane of reflexion but this only changes monotonically. The distribution, $I(\omega,2\theta)$, shows the interaction (convolution) of the various components of the diffraction process, such as the intensity distribution of the source, its spectral composition and the fragment and mosaic nature of the crystal (for the *hkl* order under study). Being two-dimensional, the distribution contains more detailed information than the one-dimensional reflexion profile

0567-7394/83/010079-05$01.50 

since, in effect, it partly deconvolutes those components which, in the traditional procedure, are projected onto one dimension. This allows a clearer recognition and appreciation of the rôles of the various components.

In addition, the study led to a recognition that, in practice, the traditional prescription for the measurement of integrated intensity contained a source of systematic error. An alternative improved prescription which eliminates this error was proposed and a procedure suggested to effect this prescription using the conventional scintillation counter – the 'slice' $\omega/2\theta$ scan procedure.*

While the essential features concerning the slice scan procedure are given in Mathieson (1982), the specific matter of the identification of peak and background is dealt with here.† It is probably best treated by reference to that distribution where there is no coordinated angular displacement of the detector with that of the crystal, *i.e.* the $\omega$ scan distribution, and where the individual (dial) settings of $\omega$ and $2\theta$ are most readily interpreted. Fig. 1 gives the distribution for the reflexion treated earlier. Instead of transforming this distribution to correspond with the distribution as it would appear in the detector aperture (Mathieson, 1982), we indicate, in Fig. 1(*a*), how a narrow aperture traverses the distribution when an $\omega/2\theta$ scan procedure is used. Operational details to be discussed later are more readily appreciated using this approach.

First it is necessary to note briefly the significance of the distribution in Fig. 1, the main features being indicated in Fig. 2(*a*). Assuming equi-axial subdivision of $\omega$ and $2\theta$ axes, the line of the fragment/mosaicity distribution, $f/m$, runs parallel to $\omega$, that of the source distribution, $s$, at an angle of ~45° (arctan 1/1) to the $2\theta$ axis and that of the spectral distribution, $\lambda$, at a corresponding angle of ~26·7° (arctan 1/2). These three distributions convoluted with one another (together with other minor factors such as the crystal size and the size of the aperture used) produce the distribution in Fig. 1. Conversely, one can, by use of a narrow slit and appropriate scan procedure (see Mathieson, 1982), extract information concerning the three main features.

On this basis, we can relate the two-dimensional distribution to different axes which are identified (*a*) with the $f/m$ distribution (coincident with the $\omega$ displacement) and (*b*) with the $\lambda$ distribution (coincident with the $\omega/2\theta$ tracking), Fig. 2(*b*). Then we can subdivide the region, $I(f/m, \lambda)$, into various parts related to these variables and consider their significance in relation to the question of peak and background. Parallel to the $\lambda$ axis is the distribution of spectral intensity and the section through the peak maximum of the $\alpha_1$ component, $f/m_0$, $\lambda_0$ (previously $\omega_0$, $2\theta_0$), provides the best estimate of this distribution, *i.e.* the line $\lambda_s$ to $\lambda_f$ (Fig. 3*a*). Parallel to the $f/m$ axis is the

* It has been pointed out by a referee that the slice scan procedure is a neat way of demonstrating the resolution function. The resolution function, *e.g.* Cooper & Nathans (1967) and later papers in the series, is generally discussed in relation to neutron diffractometers (three-crystal and two-crystal) where the components are more readily modelled as Gaussian functions. To establish the distribution experimentally in such cases, Cooper & Nathans advise the use of an additional perfect-crystal specimen. It should be noted that the neutron diffractometers involve Soller slits and use of a wide aperture in front of the detector. By contrast, our technique involves a fine-slit aperture and the two-dimensional distribution is treated in terms of operational variables, $\omega$, $2\theta$ (see Mathieson, 1982) and not in terms of reciprocal space.

† The increased resolution of this procedure is still not sufficient to deal with thermal diffuse scattering experimentally and this still requires numerical estimate of its magnitude.

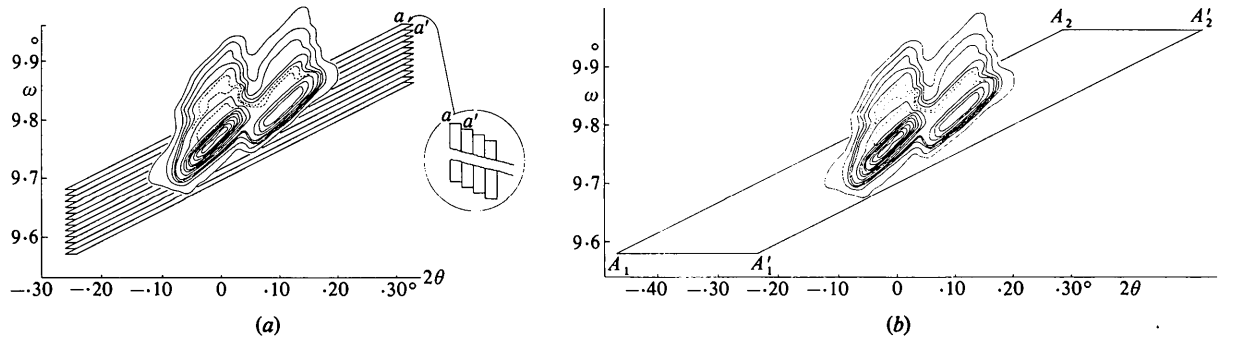


Fig. 1. The two-dimensional distribution, $I(\omega, 2\theta)$, in contour form, for an intense, low-angle ($\theta \sim 10°$) reflexion. For details of the contour levels, see Mathieson (1982). (*a*) With part of the raster of $\omega/2\theta$ slice scans which, appropriately extended in $\omega$, would cover the whole distribution. For clarity the raster is cut short of the distribution in the diagram. The aperture for the individual slice is $aa'$. The inset on the right corresponds to the slice scans transformed as in Mathieson (1982), see Fig. 5.2 (i) there. (*b*) The equivalent operation for the traditional $\omega/2\theta$ scan with a wide aperture, $AA'$. The intensity distribution along $AA'$ is combined to give a single value of intensity for the $\omega$ setting, $\omega_1$. $AA'$ traverses from $\omega_1$ ($A_1A_1'$) to $\omega_2$ ($A_2A_2'$) yielding the one-dimensional reflexion profile.

distribution of fragment/mosaicity and the section through the peak maximum ($f/m_0$, $\lambda_0$) provides the best estimate of this distribution, *i.e.* the line $f/m_1$ to $f/m_2$ (Fig. 3*b*). Any general point ($f/m$, $\lambda$) in the two-dimensional distribution corresponds to the appropriate convolution of the individual components, $f/m$ and $\lambda$, at that point, together with the effect of the source distribution. For the purposes of this discussion, the latter is relatively featureless and may be considered as having the effect of smearing, without significantly influencing the overall variations derived from the two main components.

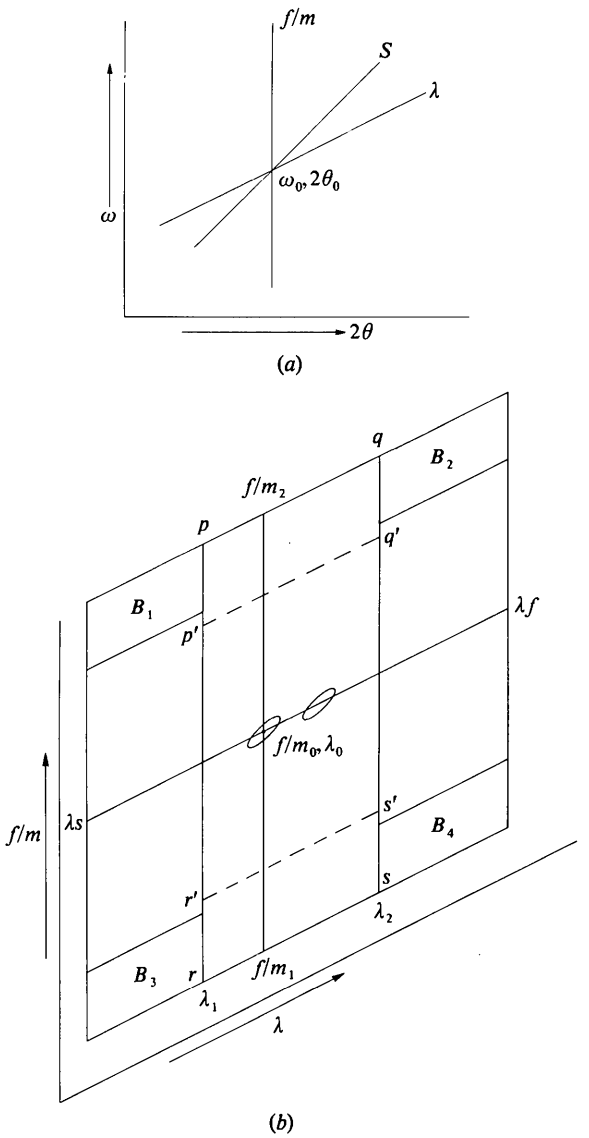


Fig. 2. (*a*) Diagram of the main features of the two-dimensional distribution. The locus of the fragment/mosaicity, $f/m$, distribution lies parallel to the $\omega$ axis while that of the source, *s*, is at an angle of ~45° (arctan 1/1) to the $2\theta$ axis and that of the spectral distribution, $\lambda$, is at an angle of ~26·7° (arctan 1/2) to the $2\theta$ axis. (*b*) The alternative choice of axes to which the distribution can be referred. One is identified with the $f/m$ distribution (coincident with the $\omega$ displacement) and the other with the $\lambda$ distribution (coincident with the $\omega/2\theta$ tracking).

By reference to the spectral curve through the peak, Fig. 3(*a*), an estimate of the magnitude of the general radiation in the wings of that curve relative to the $\alpha_1$ peak can be made. Then by reference to the parallel slice curves in the region of the wings of the $f/m$ distribution, such as Fig. 3(*c*), it is evident that the general radiation, which still retains the same proportional relationship to $\alpha_1$, is now a minor component and that the general scatter is now the major component. The general scatter components which are differentiable from the spectral curve components therefore constitute the background. These components are the main contributors to the areas $B_1$, $B_2$, $B_3$, $B_4$ in Fig. 2(*b*). Obviously, the convolutive contribution of the $f/m$ and $\lambda$ distributions can be estimated from the centre lines through $f/m_0$ and $\lambda_0$, *i.e.* Figs. 3(*b*) and (*a*) respectively, and subtracted from the corresponding values in $B_1$, $B_2$, $B_3$, $B_4$. The counts remaining in these areas will then allow an estimate of the background to be made for the area *pqrs* (say) in Fig. 2(*b*). Depending on the distribution of values in $B_1B_2B_3B_4$ being uniform or, rising towards the area *pqrs*, an appropriate correction procedure would be invoked.

For the estimation of the peak, one has to remember that the basic requirement for relative (not absolute) estimates of integrated intensity of different reflexions is that the spectral band width should be maintained constant. The $\omega/2\theta$ slice scan procedure allows this to be effected by internal reference to the $\alpha_1\alpha_2$ separation (Mathieson, 1982). On this basis, then, one can select limits $\lambda_1$ and $\lambda_2$, Fig. 2(*b*), within which estimation of the integrated intensity is made. Note that the regions $\lambda < \lambda_1$ and $\lambda > \lambda_2$ are spectral contributions and not background contributions. Here $\lambda<$ and $\lambda>$ simply mean to the left of and to the right of, respectively. True background components are associated with areas $B_1$ to $B_4$ as indicated above. So the integrated intensity in this case would be the sum of counts for points within the area, *pqrs*, less the 'background' based on the count per point of each of $B_1$, $B_2$, $B_3$ and $B_4$, scaled appropriately to the number of points in *pqrs*. This is the integrated intensity truncated within limits $\lambda_1$ and $\lambda_2$ but extending over the full range of fragment/mosaicity.

It should be noted that we are using a $\lambda$-truncated measure of integrated intensity but there is no obvious reason why the estimate of integrated intensity should not also be truncated in respect of mosaicity, say within *p'q'r's'* in Fig. 2(*b*), *provided* each reflexion is treated consistently. This does assume that the mosaic distribution for each reflexion is constant. If not, then use of the outer limit, *pqrs*, is necessary.

### Practical procedure

To carry out an $\omega/2\theta$ slice scan, certain features have to be ensured. The step in $2\theta$, $\Delta 2\theta$, should be compatible with the angular dimension of the narrow detector aperture and this determines the step in $\omega$, $\Delta\omega$. The aperture should preferably be adjustable but, in any case, it must be dimensionally stable.

Given these factors, it is advisable to carry out preliminary scans with the narrow slit aperture through the peak of the $\alpha_1$ component (say) both in $\lambda$ ($\omega/2\theta$ scan) and in $f/m$ ($\omega$ scan). Typical scans are illustrated in Figs. 3(*a*) and (*b*) respectively and provide guides as to the array to be measured and also estimates of $\lambda_1$ and $\lambda_2$, the $\lambda$ truncation limits.* It is also useful to carry out $\omega/2\theta$ slice scans near the outer $\omega$ limits of the $f/m$ distribution to assess where the distribution effectively ends; Fig. 3(*c*) illustrates a typical scan in such a region. Note that the $\alpha_1\alpha_2$ component is still clearly identified although the peak count there is only ~25 count $s^{-1}$ whereas the peak maximum, Fig. 3(*a*), is ~17 000 counts $s^{-1}$.

The effective limits of the scan in $\omega$ can be determined by reference to a signal/noise index. In the present case, the $S/N$ index for each slice scan is derived from the individual step scan counts in the following way. The 'noise', $N$, is estimated from the sum of counts between $\lambda_s$ and $\lambda_1$ and $\lambda_2$ and $\lambda_f$ and scaled to correspond to the full scan, $\lambda_s$ to $\lambda_f$, see Fig. 2(*b*). The 'signal' is then the sum of counts for the total scan less the estimated full scan 'noise'. Comparison of Fig. 3(*c*), near the outer limit of the $f/m$ distribution, with Fig. 3(*a*), at the peak, shows the change in signal to noise. Fig. 4 records the plot of $S/N$ indices. Extrapolation of the plot of $S/N$ indices (full circles) identifies effectively the limits of the scan in $\omega$. In the region of the peak, the 'noise' is largely general radiation, see Fig. 3(*a*), and not strictly background. However, as the signal drops, the 'noise' takes on its more usual connotation. Since the use of the $S/N$ indices is to establish the $\omega$ limits of the fragment/mosaicity distribution, the inaccuracy in defining noise in the high signal region is not critical for our purpose.

* (i) In Figs. 3(*a*), (*b*) and (*c*), the program identifies the maximum count and scales the other counts appropriately. The program suite used is basically that of Dr E. J. Gabe of the National Research Council of Canada and we gratefully acknowledge his making it available to us.

(ii) In Fig. 3(*a*), the open circles correspond to the amplified count scale on the right-hand side and are presented to indicate that the limits $\lambda_1$ and $\lambda_2$ can be chosen so that the $\lambda_1\lambda_2$ band width while maintained constant is relatively insensitive to exact positioning.

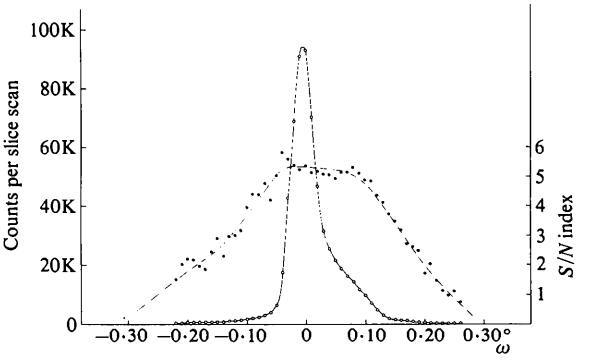


Fig. 4. Plot (open circles) of the integrated intensity components, $R$, from individual $\omega/2\theta$ slice scans at given values of $\omega$ *versus* $\omega$. Each slice scan is individually corrected for $\lambda$ truncation and 'noise' background. The signal-to-noise index, $S/N$ (full circles), is also plotted for each slice scan. Extrapolation to $S/N = 0$ establishes the true limit of the $f/m$ distribution.

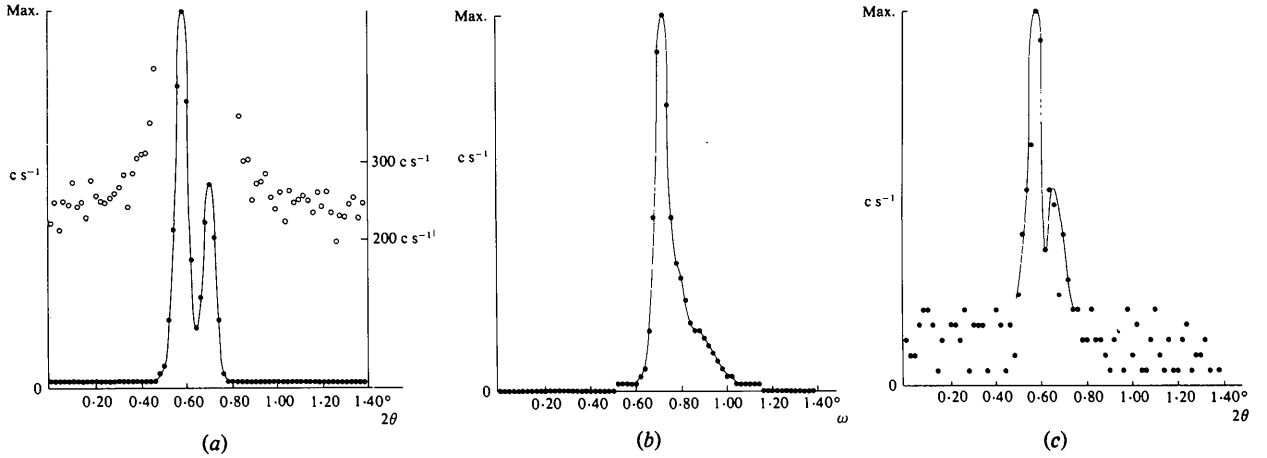


Fig. 3. Scans through the $\alpha_1$ peak; (*a*) $\omega/2\theta$ slice scan parallel to the $\lambda$ axis and (*b*) $\omega$ slice scan parallel to the $f/m$ axis. (*c*) is a typical $\omega/2\theta$ slice scan on the outer limits of the $f/m$ distribution. The maximum count is ~17 000 counts $s^{-1}$ in (*a*) and (*b*) and is 25 counts $s^{-1}$ in (*c*).

The process of data collection is relatively straightforward. Starting at the $\omega(f/m_1)$ limit, see Fig. 2(*b*), one carries out an $\omega/2\theta$ slice scan, referenced at $2\theta_0$, then moves $\Delta\omega$ and repeats the $\omega/2\theta$ slice scan with the same $2\theta$ reference. This procedure is repeated until the upper limit, $\omega(f/m_2)$, is reached. From the array of data, estimates of intensity of the peak and the background, as discussed earlier, are made and the difference deduced.

## Discussion

The experimental arrangement which yielded the distribution in Fig. 1(*a*) was simple (see Mathieson, 1982) but not grossly atypical in that some workers in the field of electron density studies have reverted to a simple set-up to minimize potential systematic error associated, for example, with correction for polarization from a monochromator crystal. Also, being simple, it establishes the basic features of the procedure and lays the foundation for exploration of more complex experimental arrangements involving (say) a position-sensitive detector or a crystal monochromator. For the neutron case, the latter situation has been examined recently with a theoretical model by Schoenborn (1982).

So far as differentiation and identification of the peak and the background, it is evident that procedures based on recognition of the known shape of a functional component of the two-dimensional distribution are objectively superior to those restricted to a low-resolution one-dimensional reflexion profile. It is obviously difficult to make a general statement at this stage as to the full capabilities of this type of procedure. Experience with a variety of crystal specimens will be needed before an estimate of improvement in accuracy (not precision) of measurement of integrated intensity can be made.

Certain comments may be offered concerning the $\lambda$ and $f/m$ distributions. Thus, for the $\lambda$ distribution, it would be advantageous to establish this on the peak of a strong reflexion and store it in memory for checking other parts of that reflexion or for checking other reflexions. Then, if multiple reflexions in general obtrude upon the distribution of a weaker reflexion, this eventuality could be detected by reference to the stored distribution and corrected or an alternative orientation chosen.

The Gaussian form of distribution is often assumed, especially for the crystal mosaicity. The evidence in Fig. 4 makes it quite clear that, in the present case, the distribution extends much further than would be consistent with a Gaussian distribution. While one may simply follow the decrease of signal with change of $\omega$ until it seems to disappear, the extent of the fragment/mosaicity distribution can be established more definitely and in an unbiased manner by extrapolation of the $S/N$ indices, see Fig. 4. It should be noted that the key diagnostics for the 'signal' are the location and shape of the $\alpha_1\alpha_2$ components in the individual $\omega/2\theta$ slice scan, see Fig. 3(*c*). The two-dimensional treatment of data indicated in Fig. 4 should have considerable value in exploring the mosaicity distribution for a range of different crystals, for purposes other than the measurement of integrated intensity.

## References

CLEGG, W. (1981). *Acta Cryst.* A**37**, 22–28.
COOPER, M. J. & NATHANS, R. (1967). *Acta Cryst.* **23**, 357–367.
LEHMANN, M. S. (1980). *Electron and Magnetization Densities in Molecules and Crystals*, pp. 295–314. New York & London: Plenum Press.
MATHIESON, A. McL. (1982). *Acta Cryst.* A**38**, 378–387.
SCHOENBORN, B. P. (1982). Submitted for publication.